IOP Conf. Series: Journal of Physics: Conf. Series **821** (2017) 012013 doi:10.1088/1742-6596/821/1/012013

SU2: the Open-Source Software for Non-ideal Compressible Flows

M. Pini[1], S. Vitale[1], P. Colonna[1], G. Gori[2], A. Guardone[2], T.Economon[3], J.J.Alonso[3], F.Palacios[4]

[1] Propulsion & Power group, Faculty of Aerospace Engineering, Delft University of Technology
[2]Department of Aerospace Science and Technology, Politecnico di Milano
[3]Aerospace Design Laboratory, Stanford University
[4]Advanced Concepts, Boeing Commercial Airplanes, The Boeing Company, Everett, United States

E-mail: m.pini@tudelft.nl

Abstract.

The capabilities of the open-source SU2 software suite for the numerical simulation of viscous flows over unstructured grid are extended to non-ideal compressible-fluid dynamics (NICFD). A built-in thermodynamic library is incorporated to account for the non-ideal thermodynamic characteristics of fluid flows evolving in the close proximity of the liquid-vapour saturation curve and critical point. The numerical methods, namely the Approximate Riemann Solvers (ARS), viscous fluxes and boundary conditions are generalised to non-ideal fluid properties. Quantities of interest for turbomachinery cascades, as loss coefficients and flow angles, can be automatically determined and used for design optimization.

A variety of test cases are carried out to assess the performance of the solver. At first, numerical methods are verified against analytical solution of reference NICFD test cases, including steady shock reflection and unsteady shock tube. Then, non-ideal gas effects in planar nozzles and past turbine cascades, typically encountered in Organic Rankine Cycle applications, are investigated and debated. The obtained results demonstrate that SU2 is highly suited for the analysis and the automatic design of internal flow devices operating in the non-ideal compressible-fluid regime.

Introduction

Non-ideal compressible fluid dynamics (NICFD) is the discipline devoted to the study of the thermo-physical characteristics of fluid flows departing from gas ideality, namely flows not obeying to the perfect gas law. Supercritical flows, dense vapors, and two-phase flows belong to this category. Due to the ever more stringent environmental regulations, the interest around non-ideal fluid flows has peaked in the propulsion and power field. For example, they are by far the essential element in Organic Rankine Cycle (ORC) turbogenerators, which are energy conversion systems renowned for the efficient exploitation of renewable energy sources [1, 2, 3, 4]. Supercritical CO_2 have become an attractive working medium for next-generation solar and nuclear power generation [5, 6] [7], as well as the key-enabler of highly-efficient refrigeration devices [8]. The successful deployment of these sustainable technologies is primarily dictated by the performance maximization of their components (e.g. turbomachinery, heat exchangers, ejectors) which can be only driven by CFD, as non-ideal flows usually exhibit gas-dynamic

phenomena largely unpredictable with simplified methods [9]. To the authors knowledge, there is currently no computational infrastructure providing analysis and design capability for non-ideal fluid flows. Robust and accurate simulations of non-ideal fluid flows is still a challenge, and the quasi-absence of experimental data in the thermodynamic regions of interest renders uncertain the reliability of the physical models embedded in CFD tools. i.e. the thermo-physical and turbulence models. Presently, several research programs are underway [10] to conduct experiments for non-ideal flow fluids aimed at providing sets of data for the validation of NICFD tools.

The SU2 software suite [11] has recently gained great interest as open-source platform for solving multi-physics PDE problems and PDE-constrained optimization problems on general unstructured meshes. The code resolves steady and unsteady Reynolds-averaged Navier-Stokes (RANS) equations for incompressible and compressible, laminar and fully turbulent, flows. As unique feature, SU2 accommodates built-in design functionalities through a continuous and a discrete adjoint solver. Therefore, equipped with accurate thermo-physical models, SU2 can eventually meet the research and industrial needs of NICFD community paving the way to unsteady design for all those applications involving non-ideal flows.

The first extension of SU2 to NICFD was thoroughly addressed in [12]. This paper documents the latest efforts undertaken by the authors to expand the capabilities towards analysis and design under non-ideal flow conditions. Especially, the thermo-physical library has been enriched by a direct coupling with the FluidProp database [13].

These new features are tested on a variety of model problems and practical applications comprising a rarefaction shock-wave over a wedge, an unsteady shock-tube, and supersonic flow within a converging-diverging nozzle and turbine vanes typical of ORC blade passages. The collection of test cases not only provides evidence of the capability of the tool but can be also considered as benchmarks for developers and users of NICFD tools.

The paper is organized as follows: section 1 reminds the governing equations for an arbitrary equilibrium real gas. Section 2 briefly recalls the adopted numerical methods. Section 3 outlines the thermo-physical models currently available in SU2, while in section 4 the obtained results are shown and discussed.

1. Governing Equations

SU2 has been designed to solve the compressible Reynolds-Averaged Navier-Stokes (RANS) equations [14], as high Mach number flows are of concern in NICFD. The system of PDE equations including the inviscid and viscous terms is usually written as

$$\partial_t \vec{U} + \nabla \cdot \vec{F}^c - \nabla \cdot \vec{F}^v = \vec{Q} \quad \text{in } \Omega,\, t > 0. \tag{1}$$

Equation (1) describes how mass, momentum and energy evolve in a control domain. $\vec{U}$ symbolizes the vector of conservative variables, i.e. $\vec{U} = (\rho, \rho v_1, \rho v_2, \rho v_3, \rho E)^\mathsf{T}$, where ρ is the fluid density, E is the total energy per unit mass, and $\vec{v} = (v_1, v_2, v_3) \in \mathbb{R}^3$ is the flow velocity in a Cartesian coordinate system. A thorough description of the model can be found in [12] and [15].

2. Numerical Algorithms

The convective fluxes are calculated by means of the Roe's approximate Riemaann solver (ARS) generalised to arbitrary fluids. As reported in [16], the averaged Jacobian matrix resulting from a local linearization of the Riemann problem (2) is no longer uniquely determined for equilibrium non-ideal flows and a new condition (3) must be satisfied.

$$\left(\vec{F}^c_{\mathrm{i}} - \vec{F}^c_j\right) = \bar{A}\left(\vec{U}_{\mathrm{i}} - \vec{U}_{\mathrm{j}}\right), \quad \bar{A} = A(\bar{\vec{U}}), \tag{2}$$

$$\bar{\chi}(\rho_{\mathrm{i}} - \rho_{\mathrm{j}}) + \bar{\kappa}(\rho_{\mathrm{i}} e_{\mathrm{i}} - \rho_{\mathrm{i}} e_{\mathrm{j}}) = (P_{\mathrm{i}} - P_{\mathrm{j}}), \tag{3}$$

where $\bar{\chi}$ and $\bar{\kappa}$ are averaged secondary thermodynamic properties defined as:

$$\chi = \left(\frac{\partial P}{\partial \rho}\right)_{\rho e} = \left(\frac{\partial P}{\partial \rho}\right)_{e} - \frac{e}{\rho}\left(\frac{\partial P}{\partial e}\right)_{\rho} \qquad , \kappa = \left(\frac{\partial P}{\partial \rho e}\right)_{\rho} = \frac{1}{\rho}\left(\frac{\partial P}{\partial e}\right)_{\rho}. \tag{4}$$

In SU2 the intermediate state is retrieved through the well-established Vinokur-Montagne' [17] approach. Second-order accuracy is achieved using a Monotone Upstream-centered Schemes for Conservation Laws (MUSCL) approach [18] with gradient limitation. The numerical viscous fluxes are conversely evaluated by averaging the flow variables, flow derivatives, and transport properties at two neighbouring cells. Characteristics based boundary conditions are enforced to the inflow/outflow boundaries. To automatically detect the incoming and outgoing waves, the approach proposed in [19] is employed. By means of an eigenvalue analysis the number of enforceable unknowns is determined and variables that can be specified at the boundary are automatically selected. For more details the reader is referred to [12].

To enhance portability, SU2 relies on widely popular open-source software for parallelization (MPI and ParMetis). More details on the parallelization paradigm can be found in [15].

3. Computation of Thermo-physical Properties

Unlike standard CFD solvers, the numerical schemes for non-ideal fluid flows require the calculation of primary and secondary, i.e. partial derivatives of primary thermodynamic variables, thermodynamic properties as a function of density ρ and internal energy e, which are in turn a recombination of the conservative variables as follows

$$\rho = U_1, \quad e = \frac{U_5}{U_1} - \frac{(U_2 + U_3 + U_4)^2}{2U_1^2} = E - \frac{\|v\|^2}{2}. \tag{5}$$

The stable equilibrium state principle assures that any other generic thermodynamic property X (e.g. pressure, temperature, etc.) is determined through an arbitrary thermodynamic model in the form

$$X = X(\rho, e) = X(\vec{U}). \tag{6}$$

Equation 6 is explicit for polytropic models, like the ideal gas (PIG), the Van der Waals (PVdW), and the Peng-Robinson (PR) available in the built-in thermodynamic library. These models ensure high computational efficiency but are not accurate approaching the critical point. However, they are useful to initialize simulations where strong non-ideal flow effects are of concern. For these latter cases, SU2 can exploit the advantages offered by the direct coupling with a general purpose thermophysical library [13] originally developed at Delft University of Technology.

4. Results and Discussion

As opposed to classic aerodynamics, no canonical test cases exist for assessing the accuracy and performance of non-ideal compressible flow solvers. Consequently, a series of numerical applications are presented thereafter, in which SU2 is first verified against known analytical solutions and then compared to results obtained by a commercial package.

4.1. Rarefaction shock-wave

In thermodynamic conditions close to the critical point fluids of complex molecules are supposed, by theory, to produce non-classical gas dynamic phenomena such as rarefaction shock waves or compression fans. The non-classical region encloses all the possible states of a thermodynamic

	Density	Pressure	Temperature	Mach
S_A	0.79	1.06	1.01	1.70
S_B	0.45	0.93	1.00	1.19

Table 1: Fluid state before and after the rarefaction shock-wave computed with SU2.

mesh tag	A	B	C	D	E	F
N elements	2301	5251	14751	49551	104351	179151
Iter time [s]	0.0145	0.03	0.086	0.4	0.6	1.3

Table 2: Number of elements composing each mesh used to discretise the domain and computational time for a single solver iteration.

system, defined as a combination of pressure, temperature and density, that produce a negative value of the *fundamental derivative of gas-dynamics* $\Gamma < 0$ [9]. For instance, linear siloxanes, synthetically denoted as MD_nM, are supposed to be endowed with this very particular region. For this family of fluids, cubic equations of state, like the Van der Waals model, admit the onset of the non-classical phenomena mentioned earlier. The fluid considered in this section is a MDM siloxane and its properties are listed in Table 3, the value of the specific heat ratio is assumed to be $\gamma = 1.0125$ for this particular test case.

The geometry consists of a simple square domain containing an edge with a design slope $\theta = 15.945°$, and the fluid flows through the domain from the left to the right boundary. Symmetry condition is applied at the upper border, while at the bottom surface an inviscid wall boundary condition is prescribed. From now on, we identify the fluid state S before the shock with the subscript A and the state S after the shock with the subscript B. Results here presented were obtained assuming fluid conditions close to the critical point to show and highlight non-classical phenomena. Convective fluxes were evaluated using an implicit, second-order accurate in space, scheme based on a standard Roe numerical scheme. Dimensionless state variables, with respect to the fluid critical values, are reported in Tab. 1 for state A and B. If the Van der Waals equation of state is used in place of the PIG law, a non-classical rarefaction shock wave occurs. Results, reported in Tab. 1, show that values of pressure and density drop across the shock. The deviation between the numerical and the theoretical value for p_B, computed using the Rankine-Hugoniot condition for a Van der Waals fluid, is approximately $5.3163 \cdot 10^{-5}\%$.

Different structured meshes, with a different level of resolution, were used to simulate the phenomenon. Tab. 2 lists the total number of elements in each mesh and the computational cost, in terms of time, of each single iteration carried out by the SU2 solver. The overall computational time is not reported here since convergence history changes significantly from mesh to mesh due to the intervention of the automatic CFL (Courant-Friedrichs-Lewy) adaptation routine. By the way, just to give an idea, the total computational time spans from roughly two hundreds seconds, for mesh A, to tens of thousands of seconds for the finer grid F.

Flow solution, reported in Fig. 1 for grid D, clearly show the presence of a non-classical rarefaction shock wave. Fig. 2 depicts Mach profiles at $y = 0.4$ along the x axis, for all the different level of space dicretisation (see Tab. 2). For grid A numerical dissipation, bound to a non adequate level of refinement, causes the shock to be smeared out over a wide portion of the domain. Trends reported in Fig. 2 show that the solution tends to converge to a shock discontinuity by increasing the level of mesh resolution. Though very small differences can still be found, Mach trends for grid E and F suggest that the solution is by now independent from the domain dicretisation. Finally, the value of the angle β, i.e. the angle between the shock and

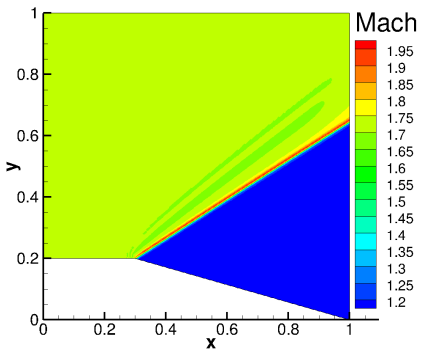

Figure 1: Van der Waals, mesh D, second order: Mach field.

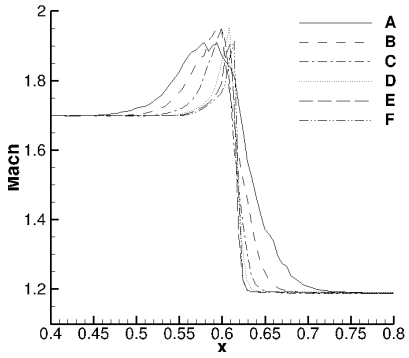

Figure 2: Mach profile along $y = 0.4$ for solution computed over different meshes.

Fluid	R_{gas} [J/KgK]	γ	P_{cr} [Pa]	T_{cr} [K]	ρ_{cr} [Kg/m^3]
Air	287.058	1.4	-	-	-
MDM	35.152	1.018	1415000	564.09	256.82

Table 3: Fluid parametes for air and MDM specified for numerical simulation of unsteady shock tube.

the direction of the x-axis, is compared against its theoretical value. The analytical relation, which depends only on the thermodynamic state of the fluid before and after the shock reads

$$\beta = \arcsin \sqrt{\frac{p_B - p_A}{\rho_B - \rho_A} \frac{\rho_B}{\rho_A} \frac{1}{c_A^2 M_A^2}}. \tag{7}$$

In the present case the analytical value is $\beta = 32.8602°$, while the computed shock angle is $\beta = 32.735°$, fairly close to the theoretical one.

4.2. 2D unsteady shock tube

The motion of a shock-wave travelling inside a pipe is presented in this section. The problem is assumed to be two-dimensional and viscous phenomena are neglected without any loss of generality. Unsteady simulation were carried out using a first order accurate dual-time stepping method. In the following, comparisons between the analytical and the numerical solution obtained by SU2 are shown. The problem is studied using both ideal and non-ideal fluids, namely air and MDM. Tab. 3 reports fluid parameters such as gas constants, critical values and specific heat ratio specified for the numerical simulations. The pipe is represented by a rectangular domain of length $L = 10$ m, along x axis, and height $h = 0.5$ m, on y axis. The shock moves from left to right and it is generated by applying a pressure and a temperature jump at the left boundary. The upper and lower boundaries are assumed to be free-slip walls. The pipe has an opening on the right boundary which allows the fluid to be discharged into an infinite-acting reservoir: a constant pressure condition is imposed here, $p_{out} = 101325$ [Pa] for air and $p_{out} = 800000$ [Pa] for MDM, is applied.

Initially, the left-to-right movement of the shock creates two uniform regions, namely 1 (upstream state with respect to the shock) and 2 (downstream state with respect to the shock). It is possible to retrieve the analytical solution of these kind of problem considering both an ideal gas or a complex fluid whose thermodynamic behaviour is characterize by means of the

	S_1	S_2	S_3	$\bar{S}_1$	$\bar{S}_2$	$\bar{S}_3$
P [Pa]	101325	130795	101325	101325	130795	101324
T [K]	303.15	326.32	303.15	303.15	326.35	303.37
ρ [Kg/m^3]	1.1644	1.3963	1.6641	1.1644	1.3961	1.1635

Table 4: Thermodynamic states retrieved through the analytical solution, and by means of numerical simulations (barred values) for air.

	S_1	S_2	S_3	$\bar{S}_1$	$\bar{S}_2$	$\bar{S}_3$
P [Pa]	800000	838120	800000	800000	838120	800000
T [K]	570.5	571.17	570.5	570.5	571.17	570.5
ρ [Kg/m^3]	49.52	52.53	49.52	49.52	52.53	49.52

Table 5: Thermodynamic states retrieved through the analytical solution, and by means of numerical simulations (barred values) for MDM.

simple, but yet qualitatively sound, Van der Waals equation of state. The so called *Rankine-Hugoniot* condition impose a relation between the pre- and the post- shock states. See [20] for the definition the Rankine-Hugoniot condition for a van der Waals fluid. Since state 1 is fully known and the value of the static pressure p_2 is chosen arbitrarily as a boundary condition, it is possible to solve Rankine-Hugoniot equation numerically to retrieve the value of the density in the post-shock region. Once ρ_2 and p_2 are available, the post-shock state is uniquely defined and the speed of the shock can be reconstructed.

After the shock is discharged through the open end, at $x = 10$ m, region 1 does no longer exist and a third region 3 arise in the domain. At the discharge section the fluid may be supersonic, transonic or subsonic leading to three different analytical solutions: only the subsonic discharge is considered hereinafter. For a subsonic discharge, a rarefaction fan is produced at the open section. Rarefaction waves travel upstream, from right to left, and generate an isentropic expansion which allows to match the outer pressure and brings to a new thermodynamic state which we will define as S_3 hereinafter. The analytical solution for this particular configuration may be retrieved by exploiting properties of Riemann invariants from characteristic theory.

The physics of the rarefaction fan for a van der Waals flow is governed by more complex equations which must account for non-ideal effects. A detailed procedure to retrieve the exact solution for a van der Waals fluid can be found in [20]. Tab. 4 and Tab. 5 report the thermodynamic states in region 1, 2, 3, respectively for air and MDM, reconstructed analytically together with their values computed through SU2 (pointed by subscript $\bar{}$). Due to the very weak shock intensity the entropy loss across the shock is negligible thus total quantities are approximately conserved, for this reason state S_3 failry matches state S_1. Figure 3 shows the analytical solution for the shock-wave travelling rightward, both for a dilute gas and for a non-ideal flow. The exact solution is compared with first and second order space accurate calculations proving that numerical results from SU2 are in good agreement with the analytical solution. The shock is correctly captured in terms of speed and intensity but the discontinuity is slightly smeared out due to numerical dissipation effects arising from space discretization and from first order time approximation.

Fig. 4 reports the same comparison for a left-ward travelling rarefaction fan. Numerical solutions, first and second order accurate in space, first order in time, are plotted against the analytical solution. The analytical solution is again correctly represented by the numerical solution.

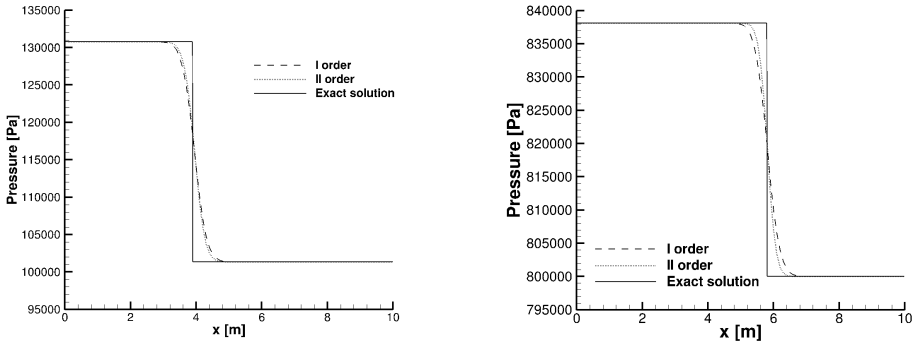

Figure 3: Comparison of the numerical against the analytical solution (continuous line). First order solution in space is represented by dashed line, second order by a dotted curve. Comparison is made at $t = 0.01$ sec for air (left) and $t = 0.05$ sec for MDM (right). The shock is moving from left to right.

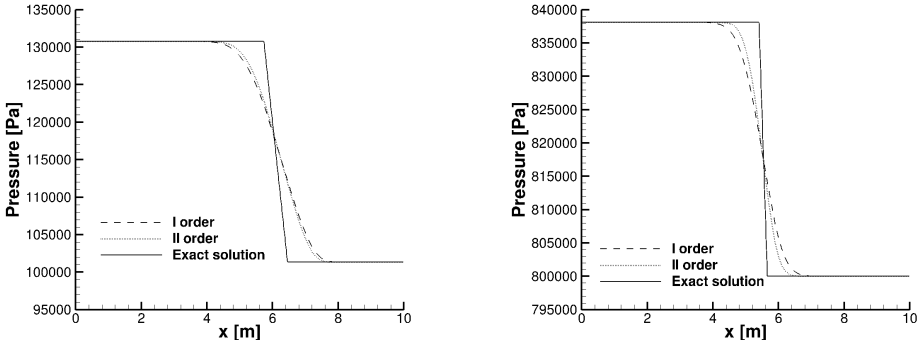

Figure 4: Comparison of the numerical against the analytical solution (continuous line). First order solution in space is represented by dashed line, second order by a dotted curve. Comparison is made at $t = 0.04$ sec for air (left) and $t = 0.13$ sec for MDM (right). The rarefaction fan is moving from left to right.

4.3. Supersonic Nozzle for Laboratory Experiments

The flow-field within a supersonic nozzle is discussed as first practical example. The nozzle is one of the test sections of the ORCHID facility, a closed-loop research rig currently under construction at Delft University of Technology [21] whose purpose is to perform fundamental studies on dense organic flows and validate NICFD tools. The test-bench is operated with siloxane MM, here modelled through the multi-parameter Span-Wagner EoS available in FluidProp. Table 6 summarizes the input parameters for this simulation. Results provided by the commercial package Ansys-CFX [22] are used for verification purposes. In both cases the Navier-Stokes equations were solved using an implicit Euler algorithm based on CFL adaptation. Note that in CFX the MM properties are available in tabulated form, which makes the computational cost of the single iteration of CFX about 50% lower than that of SU2 on four Intel i7-3630QM CPU 2.4 GHz physical cores. Figures 5 and 6 display the Mach contour and the pressure distribution along the nozzle mid section respectively. The results fairly well correlate, suggesting that, though missing experimental confirmation, SU2 can be adopted for simulating NICFD flows in practical applications.

Total inlet temperature	257.0 $^{\circ}C$
Total inlet pressure	18.423 bar
Static back-pressure	2.0 bar
Turbulence model	SST-kω
Inlet turbulence intensity	0.05
Space discretization (SU2)	Upwind generalized Roe 2nd order
Space discretization (CFX)	High resolution method

Table 6: Input parameters for the supersonic nozzle test case.

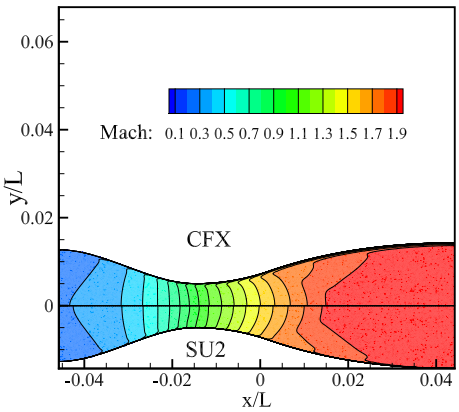

Figure 5: Mach contour at the mid section of the nozzle.

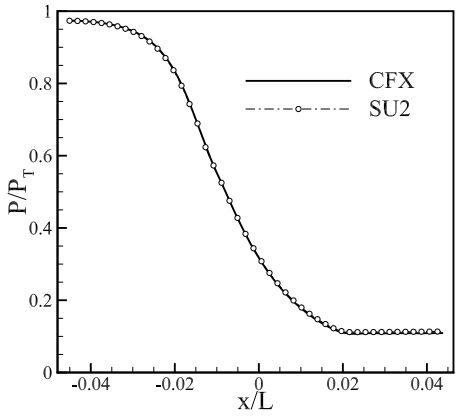

Figure 6: Streamwise distribution of the static pressure at the mid section of the nozzle.

4.4. Supersonic ORC Blade Passage

The last test case is representative of stator vanes of single-stage axial ORC expanders. As pointed out in [23], the passage was designed by resorting to oversimplified flow models and was recently used to assess the effectiveness of shape optimization for highly non-ideal flows [24]. The turbine is operated with the siloxane MDM modelled by the polytropic improved Peng-Robinson-Stryjek-Vera equation of state. Three structured grids of increasing density level (with two cells in span-wise direction) are used for the calculations. The SST-kω turbulence model is used ensuring wall $y+$ well below the unity all along the blade surface. As only blade-to-blade flow features are of interest, free-slip conditions are imposed on the endwalls, and periodicity is set on the upper and the lower boundaries. A summary of the input parameters for the simulation can be found in Table 7. As in the previous case, SU2 simulations are verified against the results provided by the Ansys-CFX solver. Again, in both cases the equations were solved using an implicit Euler algorithm based on CFL adaptation. At first, a mesh sensitivity study is carried out to gain insight of the convergence rate of the two solvers. The mass-averaged entropy loss coefficient $Y = \frac{S_{in}-S_{out}}{S_{in}}$ is considered as merit function for the study. It is worth mentioning that this quantity is automatically computed by SU2 at runtime. Figure 9 shows the variation of such coefficient for increasing mesh sizes. As can be observed, the two solvers exhibit similar convergence properties, the solution being mesh-independent for grids finer than 200k cells. The calculation with SU2 on the coarsest grid reached full convergence after 200

Total inlet temperature	272 $°C$
Total inlet pressure	8 bar
Static back-pressure	1.0 bar
Inlet turbulence intensity	0.05
Space discretization (SU2)	Upwind generalized Roe 2nd order
Space discretization (CFX)	High resolution method

Table 7: Input parameters for the supersonic ORC blade passage.

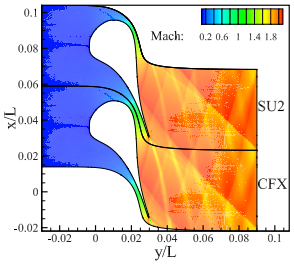

Figure 7: Mach contour.

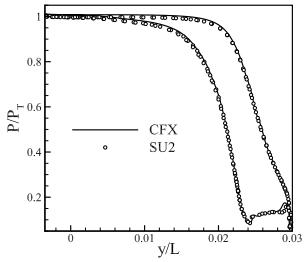

Figure 8: Pressure distribution along the blade surface.

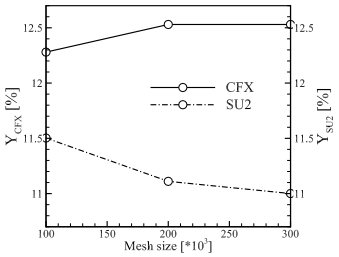

Figure 9: Mesh sensitivity study.

iterations (about 250 seconds on four Intel i7 - 2.2 GHz physical cores). Figure 7 displays the Mach number contour obtained by the two solvers for the finest grid. As expected, two shock waves are generated at the blade trailing edge, forming the so-called fishtail shock configuration. The trailing-edge shock from the pressure side is reflected on the suction side of the successive blade, while the suction-side trailing shock propagates downstream towards the outlet. At approximately $y/L = -0.06$ the two shocks coalesce into a single, stronger shock wave traveling downstream. Such interaction is somehow more visible in the SU2 solution, which is therefore found to capture these flow features more accurately.

5. Conclusions

In this paper, the capability of SU2 for simulating non-ideal compressible flows were illustrated and demonstrated through model problems and practical examples.

The results showed that, equipped with complex equations of state and appropriate numerical schemes, SU2 can be successfully used to predict non-classical gas dynamic phenomena such as rarefaction shock waves. The numerical outcomes furthermore indicated that SU2 is highly suited for the analysis of both steady and unsteady flows in the non-ideal compressible flow regime. Moreover, the novel integrated turbomachinery features makes the tool attractive for automated design of two and three-dimensional ORC turbine cascades and, more in general, of internal flow devices operating in the vicinity of the critical point.

Current developments are devoted to implement look-up tables to further enhance computational efficiency and to multi-row turbomachinery calculations for analysis and design purposes.

6. Acknowledgements

Matteo Pini and Salvatore Vitale would like to acknowledge the STW and Dana Spicer on the CC-Powertrain project. Alberto Guardone and Giulio Gori would like to acknowledge the

European Research Council (ERC) of the European Research Council Executive Agency.

References

[1] Drescher, U., and Bruggeman, D., 2007. "Fluid selection for the Organic Rankine Cycle (ORC) in biomass power and heat plants". *Applied Thermal Engineering,* ***27***(1), pp. 223–228.

[2] Lang, W., Almbauer, R., and Colonna, P., 2013. "Assessment of Waste Heat Recovery for A Heavy-duty Truck Engine Using An ORC Turbogenerator". *Journal of Engineering for Gas Turbines and Power-Transactions of the ASME,* ***135***(4), pp. 042313–1–10.

[3] Quoilin, S., Broek, M. V. D., Declaye, S., Dewallef, P., and Lemort, V., 2013. "Techno-economic survey of Organic Rankine Cycle (ORC) systems". *Renewable and Sustainable Energy Reviews,* ***22***(0), pp. 168–186.

[4] Casati, E., Vitale, S., Pini, M., Persico, G., and Colonna, P., 2014. "Centrifugal Turbines for Mini-Organic Rankine Cycle Power Systems". *Journal of Engineering for Gas Turbines and Power,* ***136***, pp. 122607–1–11.

[5] Lettieri, C., Baltadjiev, N., Casey, M., and Spakovszky, Z., 2014. "Low-Flow-Coefficient Centrifugal Compressor Design for Supercritical CO_2". *Journal of Turbomachinery,* ***136***, pp. 081008–1–9.

[6] Lettieri, C., Yang, D., and Spakovszky, Z., 2014. "An Investigation of Condensation Effects in Supercritical Carbon Dioxide Compressors". In The 4th International Symposium - Supercritical CO_2 Power Cycles.

[7] Dostal, V., Hejzlar, P., and Driscoll, M., 283-301. "The supercritical carbon dioxide power cycle: comparison to other advanced power cycles". *Nuclear technology,* ***154***(3).

[8] Elbel, S., 2011. "Historical and present developments of ejector refrigeration systems with emphasis on transcritical carbon dioxide air-conditioning applications". *International Journal of Refrigeration,* ***34***(7), 11, pp. 1545–1561.

[9] Colonna, P., and Guardone, A., 2006. "Molecular interpretation of nonclassical gas dynamics of dense vapors under the van der Waals model". *Physics of Fluids,* ***18***, pp. 056101–14.

[10] Guardone, A., Spinelli, A., and Dossena, V., 2013. "Influence of Molecular Complexity on Nozzle Design for an Organic Vapor Wind Tunnel". *ASME Journal of Engineering for Gas Turbines and Power,* ***135***.

[11] Palacios, F., Colonno, M. R., Aranake, A. C., Campos, A., Copeland, S. R., Economon, T. D., Lonkar, A. K., Lukaczyk, T. W., Taylor, T. W. R., and Alonso, J. J., 2013. "Stanford University Unstructured (SU^2): An open-source integrated computational environment for multi-physics simulation and design". *AIAA Paper 2013-0287,* ***51st AIAA Aerospace Sciences Meeting and Exhibit***, January.

[12] Vitale, S., Gori, G., Pini, M., Guardone, A., Economon, T. D., Palacios, F., Alonso, J. J., and Colonna, P., 2015. "Extension of the su2 open source cfd code to the simulation of turbulent flows of fluids modelled with complex thermophysical laws". *AIAA Paper,* ***2760***, p. 2015.

[13] Colonna, P., and van der Stelt, T., 2005. FluidProp: A program for the estimation of thermo-physical properties of fluids. Tech. rep.

[14] Landau, L., and Lifshitz, E., 1993. *Fluid Mechanics (2nd Edition).* Pergamon Press.

[15] Economon, T. D., Mudigere, D., Bansal, G., Heinecke, A., Palacios, F., Park, J., Smelyanskiy, M., Alonso, J. J., and Dubey, P., 2016. "Performance optimizations for scalable implicit {RANS} calculations with {SU2}". *Computers & Fluids,* ***129***, pp. 146 – 158.

[16] Cinnella, P., 2006. "Roe-type schemes for dense gas flow computations". *Computers & Fluids,* ***35***(10), pp. 1264–1281.

[17] Montagne, J., and Vinokur, M., 1990. "Generalized flux-vector splitting and Roe average for an equilibrium real gas". *Journal of Computational Physics,* ***89***(2), pp. 276–300.

[18] van Leer, B., 1979. "Towards the ultimate conservative difference scheme V. a second-order sequel to Godunov's method". *Journal of Computational Physics,* ***32***(1), July, pp. 101–136.

[19] Guardone, A., Isola, D., and Quaranta, G., 2011. "Arbitrary Lagrangian Eulerian formulation for two-dimensional flows using dynamic meshes with edge swapping". *Journal of Computational Physics,* ***230***(20), pp. 7706–7722.

[20] Quartapelle, L. P., Castelletti, Guardone, A., and Quaranta, G., 2003. "Solution of the Riemann problem of classical gasdynamics". *Journal of Coputational Physics,* ***190***, p. 2003.

[21] Head, A. J., De Servi, C., Casati, E., Pini, M., and Colonna, P., 2016. "Preliminary design of the ORCHID: a facility for studying non-ideal compressible fluid dynamics and testing ORC expanders". In ASME Turbo Expo 2016, no. GT2016-56103.

[22] ANSYS Inc. Academic Research, R. ., 2012. *CFX.*

[23] Colonna, P., Harinck, J., Rebay, S., and Guardone, A., 2008. "Real-gas effects in organic rankine cycle turbine nozzles". *Journal of Propulsion and Power,* ***24***(2), pp. 282–294.

[24] Pini, M., Persico, G., Pasquale, D., and Rebay, S., 2015. "Adjoint method for shape optimization in real-gas flow applications". *Journal of Engineering for Gas Turbines and Power,* ***137***(3), p. 032604.